

# Whole-Body Specific Absorption Rate Assessment of Lossy Objects Exposed to a Diffuse Field Inside a Reverberant Environment

Damir Senic, *Member, IEEE*, Antonio Sarolic, *Member, IEEE*, Christopher L. Holloway, *Fellow, IEEE*, and John M. Ladbury, *Member, IEEE*

**Abstract**—In this study, we provide a novel approach for exposure assessment in terms of whole-body average specific absorption rate (WBSAR) due to the electromagnetic fields inside reverberant environments. The approach utilizes *power balance theory* and the lossy object's absorption cross section (ACS). We use this to present a noninvasive technique for determining the WBSAR in reflective environments. Measurements were performed inside a reverberation chamber on spherically-shaped phantoms filled with lossy liquids. The approach was verified by performing invasive temperature measurements and showed excellent agreement (within 5%). This approach can be used for human exposure assessment inside reverberant environments since human body ACS has been well studied in the literature. The main advantage of the proposed approach is that it overcomes the need for complex invasive measurements in order to determine WBSAR.

**Index Terms**—Absorption cross section (ACS), dosimetry, exposure assessment, microwave measurement, reverberation chamber, specific absorption rate (SAR).

## I. INTRODUCTION

IN THIS study, we present a novel approach for exposure assessment of lossy objects (potentially including humans) exposed to radio frequency (RF) electromagnetic fields in reverberating indoor environments. The approach is based on *power balance theory* [1] and requires knowledge of the environment's quality ( $Q$ ) factor and the exposed object's absorption cross section (ACS).

The study was motivated by the lack of methods in relevant standards for human exposure assessment due to the RF electromagnetic fields inside reverberant environments. Exposure assessment guidelines [2], [3] generally assume uniform, plane-wave exposure in free-space, which cannot be applied to all real exposure situations. Humans are often exposed inside

Manuscript received June 22, 2016; revised October 7, 2016; accepted November 6, 2016. Date of publication November 24, 2016; date of current version March 15, 2017. This work was supported in part by the U.S. Government, not protected by U.S. copyright, and in part by the Ministry of Science, Education and Sports of the Republic of Croatia under Research Project 023-0000000-3273 "Measurements in EMC and EM health effects research."

D. Senic, C. L. Holloway, and J. M. Ladbury are with the Communications Technology Laboratory, National Institute of Standards and Technology, Boulder, CO 80305 USA (e-mail: Damir.Senic@nist.gov; Christopher.Holloway@nist.gov; John.Ladbury@nist.gov).

A. Sarolic is with the Chair of Applied Electromagnetics, FESB, University of Split, Split 21000, Croatia (e-mail: Antonio.Sarolic@fesb.hr).

Color versions of one or more of the figures in this paper are available online at <http://ieeexplore.ieee.org>.

Digital Object Identifier 10.1109/TEM.2016.2626968

indoor environments to RF fields coming from all directions. Hence, indoor environments can be considered reverberant with different  $Q$  factor values. Therefore, we present an approach which takes into consideration environment characteristics defined in terms of  $Q$  factor for the proper exposure assessment.

Previous work involving reverberation chambers for human exposure assessment can be found in [4]–[6]. The approach given in [4]–[6] was based on the chamber decay time and *room acoustics theory* [7] adapted for electromagnetic studies (*room electromagnetics*).

This paper is organized as follows. Bio effects due to RF electromagnetic exposure along with exposure assessment studies are presented in Section II. Section III follows with the measurement setup and techniques used to assess the exposure in terms of whole-body average specific absorption rate (WBSAR). In Section IV, we evaluated the reverberation chamber in terms of parameters that impact the uncertainty: number of uncorrelated mode-stirring samples, spatial uniformity, and Rician  $K$  factor. Exposure assessment results gathered from two different approaches are presented in Section V. A measurement uncertainty budget is given in Section VI. Final conclusions are found in Section VII.

## II. BIO EFFECTS OF RF EM FIELDS

Generally, we can state that biological effects occur when any physiological change can be observed in biological tissue exposed to electromagnetic fields [8]. Potential adverse effects could arise from situations where physiological change exceeds upper limits that tissues are able to compensate for.

It is commonly known that in the RF range biological tissues act as electrolyte solution containing polar molecules. RF fields interact with a biological tissue through ionic conduction and forced rotation of polar water molecules. In this way, absorbed RF energy is transformed into molecular kinetic energy causing a heating effect of the irradiated tissue. Hence, tissue heating is considered a primary bioeffect at RF frequencies, where tissue temperature rises despite its thermoregulatory process. If the tissue experiences heat, caused by an external source, at a rate much higher than the system's ability to compensate, thermal damage may occur.

Biological systems tend to change their functions according to temperature change. Heating processes due to RF exposure can result in adverse health effects such as cataracts,

increased blood pressure, dizziness, weakness, disorientation, and nausea [8].

Specific absorption rate (*SAR*) is a measure of the rate at which energy is absorbed by a biological system when exposed to RF electromagnetic fields [8].

International Commission on NonIonizing Radiation Protection (ICNIRP) guidelines [2] propose electric field, magnetic field, current density, and power density exposure limits. These limits are based on the established short-term adverse effects of electromagnetic radiation, which are essentially given as the stimulation of muscle and nervous tissue cells and tissue heating effects. These effects can be quantitatively presented by the induced current density (*J*) and the *SAR*. Limiting values of *J* and *SAR* are given in ICNIRP guidelines as the basic restrictions, which implies that these values are directly associated with an adverse effects that arise from the electromagnetic radiation interaction with a human body.

#### A. Exposure Assessment Based on Bioheat Equation

*SAR* is a quantity that cannot be easily measured in practice, but can be determined theoretically or empirically through models. It can also be expressed in terms of specific absorption (*SA*) as the time derivative of incremental energy *dW* absorbed by incremental mass *dm* in infinitesimal volume element *dV* of a given density  $\rho$  [8]:

$$SAR = \frac{dSA}{dt} = \frac{d}{dt} \frac{dW}{dm} = \frac{d}{dt} \frac{dW}{\rho dV}. \quad (1)$$

Electromagnetic energy deposition in lossy objects causes a temperature rise; therefore, *SAR* presents the measure of this heating effect and can be expressed by

$$SAR = c \frac{dT}{dt} = c \left. \frac{\Delta T}{\Delta t} \right|_{\Delta t \rightarrow 0} \quad (2)$$

where *c* is the specific heat capacity, *T* is the temperature, and *t* is the time period. Temperature rise in lossy dielectrics is determined by power *P* dissipated into heat. This power averaged over volume *V* equals

$$\frac{P}{V} = E \cdot J^* = \sigma E \cdot E^* = \sigma |E|^2 \quad (3)$$

where *J* is the current density, *E* is the electric field induced in a lossy dielectric, and  $\sigma$  is its conductivity. By substituting (3) into (1), the *SAR* is given by

$$SAR = \frac{dP}{dm} = \frac{dP}{\rho dV} = \frac{\sigma}{\rho} |E|^2 \quad (4)$$

where we used the fact that  $dW/dt = P$ .

Expression (2) is valid only at the very beginning of exposure, or when thermal conduction, convection, and radiation (heat transfer mechanisms) are negligible. Our experimental setup is based on the use of nonbiological homogeneous objects suspended in (and surrounded by) air, causing the loss of heat through convection. Other heat transfer mechanisms can be neglected in this case. Therefore, the temperature change can be described by the bioheat transfer equation [3], [9] reduced to

$$H_{EM} - H_{conv} = \rho c \frac{\partial T}{\partial t} \quad (5)$$

where  $H_{EM}$  is the RF radiation heat source term given by

$$H_{EM} = \rho \cdot WBSAR = \sigma |E|^2 \quad (6)$$

and  $H_{conv}$  is the convection heat rate per unit volume, given by [10]

$$H_{conv} = hA(T_2 - T_1)/V \quad (7)$$

where *h* is the convection heat transfer coefficient, *A* is the surface area between two media at different temperatures, *V* is the object's volume, and  $T_1$  and  $T_2$  are the surrounding medium and observed object temperature, respectively. Substituting (6) and (7) into (5), we obtain the expression for *SAR* measured by mean temperature rise of a lossy dielectric over an observed time period

$$SAR = \frac{hA}{\rho V} (T_2 - T_1) + c \frac{\partial T}{\partial t}. \quad (8)$$

#### B. Exposure Assessment Based on Power Balance Theory

Lossy objects exposed to RF radiation absorb electromagnetic energy that causes the heating effect which could lead to the harmful biological effect. Lossy object exposure can occur in very different situations, including reverberant, indoor environments. Such environments exhibit an internal modal structure similar to that found in reverberation chambers [1].

Reverberation chambers commonly deploy relative measurements of scattering (*S*) parameters for the empty and loaded chamber, where transmitting and receiving antennas should be placed inside the chamber at least a half-wavelength apart from any obstacle. Antennas should be aimed away from each other in order to lower the direct energy coupling (*K* factor) between them. It is necessary to have a low *K* factor due to the fact that a high *K* factor results in lack of spatial uniformity (*SU*) and high measurement uncertainty [11]–[13]. Power measured by the receiving antenna in an empty chamber differs from the power measured by the same antenna in a chamber loaded by lossy objects. That power difference equals exactly the power that was absorbed by the lossy objects. Taking this analysis a step further, we can derive the expression for the exposure assessment inside reverberant environments given in terms of the *WBSAR* [14], [15] as

$$WBSAR = \frac{\langle P_{abs} \rangle}{m} = \frac{\langle P_{r,empty} \rangle - \langle P_{r,loaded} \rangle}{m} \quad (9)$$

where brackets denote an ensemble average over all stirrer orientations,  $P_{abs}$  is the power absorbed by the lossy object,  $P_{r,empty}$  is the power received by the receiving antenna for the empty chamber,  $P_{r,loaded}$  is the power received by the receiving antenna for the loaded chamber, and *m* is the objects' mass.

The presence of lossy objects generally impacts the environment *Q* factor [1]. The above defined two powers can be calculated from associated *Q* factors for the empty and loaded chamber, respectively

$$\langle P_{r,empty} \rangle = \frac{\lambda^3}{16\pi^2 V} P_t Q_{empty} \quad (10)$$

$$\langle P_{r,loaded} \rangle = \frac{\lambda^3}{16\pi^2 V} P_t Q_{loaded} \quad (11)$$

where  $P_t$  is the transmitted power,  $\lambda$  is the wavelength, and  $V$  is the chamber's volume. Empty chamber  $Q_{\text{empty}}$  can be either estimated by knowing the room characteristics or can be directly measured. The loaded chamber  $Q_{\text{loaded}}$  can be determined from the empty chamber  $Q_{\text{empty}}$  and the  $Q$  factor associated with the lossy objects ( $Q_{\text{abs}}$ ) as

$$Q_{\text{loaded}}^{-1} = Q_{\text{empty}}^{-1} + Q_{\text{abs}}^{-1} \quad (12)$$

where  $Q_{\text{abs}}$  can be calculated from the objects' ACS as

$$Q_{\text{abs}} = \frac{2\pi V}{\langle ACS \rangle \lambda}. \quad (13)$$

Thus, the following method for estimating *WBSAR* is based on the knowledge of the exposed lossy objects' ACS

$$WBSAR = \frac{P_t \lambda^3}{16\pi^2 m V} \frac{Q_{\text{empty}}^2}{Q_{\text{empty}} + \frac{2\pi V}{\langle ACS \rangle \lambda}}. \quad (14)$$

Prior work on the ACS of different lossy objects, including human bodies in different postures, can be found in [15]–[21].

### III. MEASUREMENT SETUP

A reverberation chamber was used to determine a lossy object's *WBSAR* based on *power balance theory* and ACS. Validation measurements, based on the bioheat equation, were also performed inside the reverberation chamber. Therefore, we prepared two different measurement setups. The first one, for *power balance theory* based *WBSAR* assessment, used  $S$  parameter measurements gathered by a Vector Network Analyzer (VNA). From the  $S$  parameters, we calculated the object under test's (OUT) ACS which was used to obtain *WBSAR* (14). A detailed description of this measurement setup with ACS results can be found in [16]. The second setup (validation) was prepared to access *WBSAR* from the bio-heat (8) and deployed a signal generator with a power amplifier to generate high-field levels and a thermometer to measure the temperature rise in the exposed OUTs. The schematic layout of the validation measurement setup is shown in Fig. 1.

The chamber was made of aluminum having dimensions: ( $L$ ) 1.49 m  $\times$  ( $W$ ) 1.16 m  $\times$  ( $H$ ) 1.45 m. According to [22] and [23], this size chamber enables measurements starting at approximately 1 GHz. The chamber was equipped with a single aluminum mechanical stirrer mounted between the ceiling and the floor. The stirrer rotated about a vertical axis within a cylindrical volume 1.1 m in height and 0.6 m in diameter. Broadband (1–18 GHz) double-ridged horn antennas were used as transmitting and receiving antennas. Antennas were aimed away from each other to reduce the direct (unstirred) energy coupling between them.

We used three different OUTs for the reference measurements. The first one was a water-filled sphere in a PVC shell with 15 cm diameter (large shell), the second one was the same 15 cm sphere filled with a broadband head simulating liquid (HSL) [24], and the third was a water-filled sphere in a glass shell with 10 cm diameter (small shell). All OUTs were placed within the chamber's working volume (more than  $\lambda/2$  away from any obstacle) where the average field is expected to have

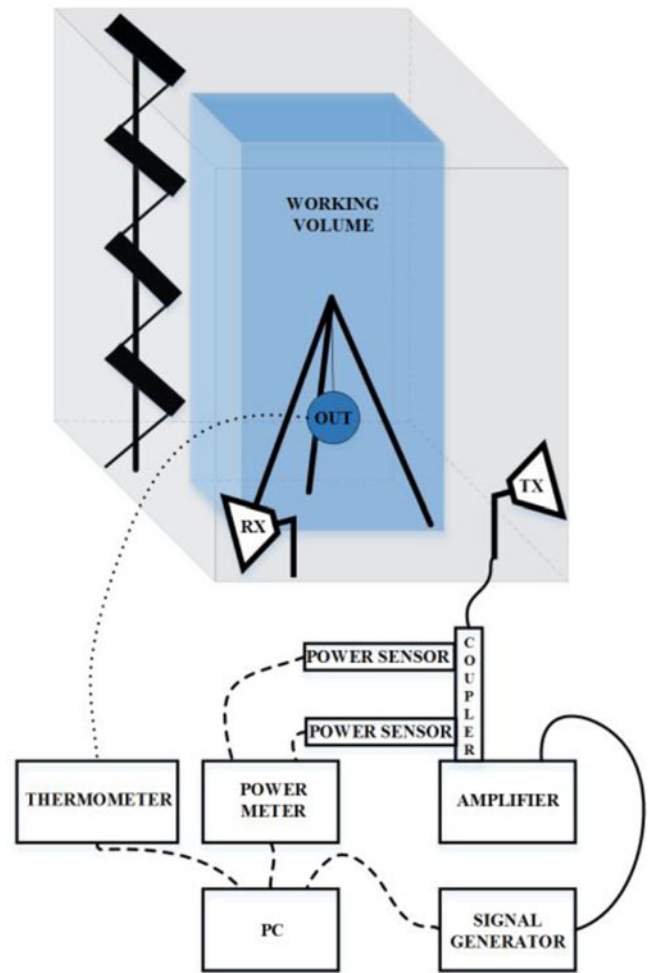


Fig. 1. Schematic layout of the validation measurement setup.

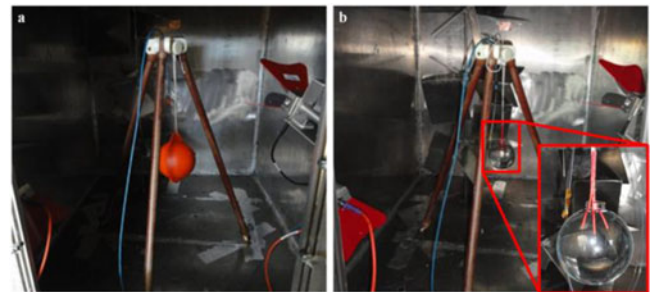


Fig. 2. Reverberation chamber interior for both power balance theory and bio-heat based measurements. (a) water- and HSL-filled large shell. (b) Water-filled small shell.

a statistically-uniform distribution. The environment inside the reverberation chamber is shown in Fig. 2.

Exposure assessment based on *power balance theory* relies on the known OUT's ACS, which can be found in [16]. In this paper, we will not focus on the OUTs ACS measurement, but will use the final results from [16].

To assess the exposure using the bioheat equation, we needed to measure the temperature rise inside the OUTs during the

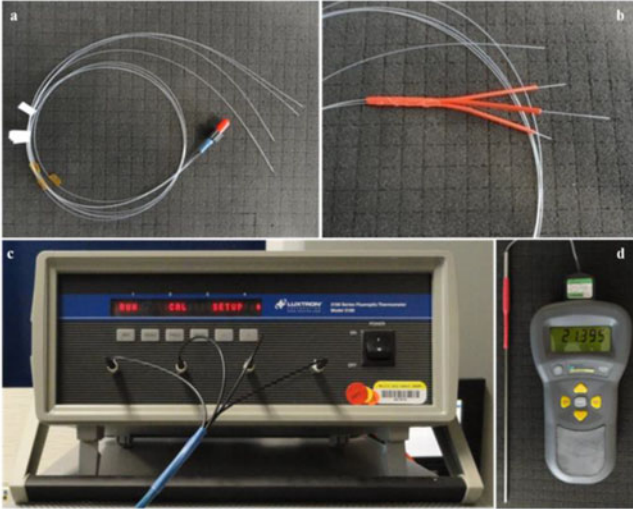


Fig. 3. Temperature measurements. (a) Fluoroptic probes. (b) Probe arrangement that enables temperature spatial measurements. (c) Four-channel fluoroptic thermometer [25]. (d) Reference thermometer [26].

exposure time. The temperature rise inside the lossy object exposed to the high-field levels was measured for each single OUT placed inside the chamber.

A CW signal was generated by a signal generator and amplified by a nominal 50-W amplifier in order to achieve a high-strength field capable of causing a noticeable temperature rise in the observed lossy object. The temperature rise was monitored over a 2-h period at 60 different paddle positions (2 minutes per paddle position) and at four discrete frequencies: 1, 1.8, 2.45, and 3 GHz. Input and reflected powers into the chamber were monitored, through a directional coupler, with power sensors connected to a power meter. Temperature rise was measured by a four-channel fluoroptic thermometer with four optical probes shown in Fig. 3(a)–(c) [25]. Three probes were immersed inside the OUT, enabling spatial averaging of measured temperature [see Figs. 2(b) and 3(b)]. One probe was left outside the OUT to monitor the chamber’s ambient temperature, which was required for determining the convection heat transfer coefficient. The temperature was measured every 5 s, yielding 1440 temperature measurement points in a 2-h period. Prior to each measurement, all four probes were calibrated in a water bath whose temperature was measured with a highly accurate reference thermometer, as shown in Fig. 3(d) [26].

#### IV. CONFIGURING THE REVERBERATION CHAMBER

The chamber configuration generally has a significant effect on the measurement uncertainty of the metrics that we are trying to estimate. For tests involving reverberation chambers, we want to configure the chamber in such a way that the errors in observed quantities are as low as possible. Parameters that we are studying here and that impact overall uncertainty includes mode-stirring sequence, spatial uniformity, and type, location, and orientation of the antennas used inside the chamber.

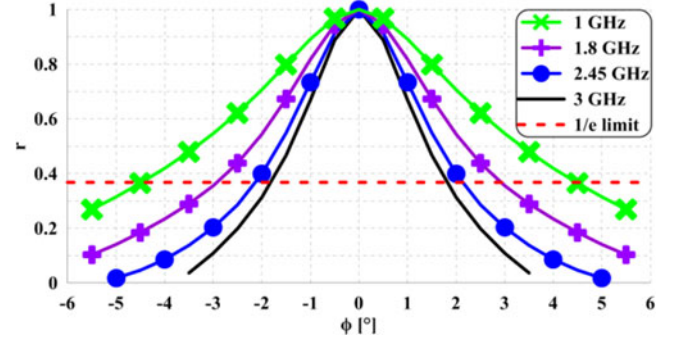


Fig. 4. Correlation between different paddle orientations calculated at three different frequencies and compared to the  $1/e$  limit.

#### A. Number of Uncorrelated Mode-Stirring Samples

In order to evaluate a reverberation chamber’s performance, the number of independent samples that a stirrer can provide needs to be determined. At each observed frequency, the stirrer must efficiently change the boundary conditions to produce a statistically significant variation of the field distribution inside the chamber. Samples taken in statistically significant different conditions are considered as statistically independent. Existence of correlation among the measurements performed in a reverberation chamber severely influences the efficiency of the measurement procedure.

To calculate the number of uncorrelated paddle orientations, we performed measurements at 720 stirrer orientations ( $0.5^\circ$  paddle step). The circular autocorrelation was computed [27] at four different frequencies of interest as follows:

$$r = \frac{\langle S_{21n}(f_m) S_{21n+\Delta n}^*(f_m) \rangle_n - |\langle S_{21n}(f_m) \rangle_n|^2}{\langle |S_{21n}(f_m)|^2 \rangle_n - |\langle S_{21n}(f_m) \rangle_n|^2}, \quad (15)$$

where we use the complex  $S_{21}$  parameter at the  $m$ -th frequency point  $f_m$  and  $n$ th stirrer orientation. The obtained coherence angle ( $\phi$ ) equals  $\sim 9^\circ$  at 1 GHz,  $\sim 5.6^\circ$  at 1.8 GHz,  $\sim 4.5^\circ$  at 2.45 GHz, and  $\sim 3.6^\circ$  at 3 GHz, with a  $1/e$  threshold [22] (see Fig. 4). We use the coherence angle to estimate the total number of uncorrelated measurements ( $N_{\text{est}}$ ) that may be achieved [28]–[30] as  $N_{\text{est}} = 360^\circ/\phi$ . In our case, the calculated coherence angle would result in 40 uncorrelated measurements at 1 GHz, 64 at 1.8 GHz, 80 at 2.45 GHz, and 100 at 3 GHz.

#### B. Spatial Uniformity

$SU$  is an important metric in reverberation chamber measurements. It provides information about the field homogeneity inside the chamber, which is required for electromagnetic compatibility (EMC) testing. The  $SU$  was determined according to [22]. The data were collected with the receiving antenna at eight ( $i = 1, 2, \dots, 8$ ) different locations that form the corners of the working volume, while the transmitting antenna was kept at a fixed location.

$SU$  was expressed in terms of the standard deviation of the normalized transmission factor for three different polarizations ( $j = 1, 2, 3$ ) and the total data set. The total data set was represented by 24 measurements gathered by combining the

three individual polarization components at the eight measurement locations. The standard deviation for our chamber loaded by different OUTs was  $\sim 1.4$  dB at all four frequencies of interest.

### C. Rician $K$ factor

In the ideal reverberation chamber, all energy that comes to the receiving antenna is well stirred (diffuse energy) and there is no direct coupling between transmitting and receiving antennas. Real situations are a bit different and direct coupling between the antennas exists. A metric which is used to quantify the direct energy coupling is the Rician  $K$  factor. The  $K$  factor is generally defined as the ratio of unstirred ( $P_u$ ) and stirred power ( $P_s$ ) and can be estimated from the  $S$ -parameters [31]:

$$K = \frac{|\langle S_{21} \rangle_N|^2}{\langle |S_{21} - \langle S_{21} \rangle|^2 \rangle_N}. \quad (16)$$

Since direct energy coupling between antennas is generally undesirable in reverberation chamber measurements, the  $K$  factor should be as low as possible for EMC tests. Prior work on the  $K$  factor in reverberation chamber measurements can be found in [11], [31]–[35].

The  $K$  factor depends on several different factors including antenna type, location, and orientation, and the chamber's loading. Here, we considered a chamber loaded with different OUTs and fixed antenna orientations, i.e., aimed away from each other and cross polarized, which yields the lowest  $K$  factor. Another common method for reducing the coupling includes placing a shield between the antennas. The measured  $K$  factor at all four frequencies of interest was, on average, lower than  $-15$  dB, indicating that the unstirred component was 30 times lower than the stirred one.

## V. ASSESSMENT OF RESULTS

$WBSAR$  may be computed from a measured temperature rise due to a high-field exposure from (8). Even though power levels were much higher ( $\sim 50$  W), all exposure measurements were normalized to 1 W of transmitted power. The measurement setup produced a temperature rise of several degrees. However, the results are presented as normalized due to the fact that the transmitted power varied with frequency.

The water temperature was measured with three probes, and their average chosen as the measurement result. The temporal temperature rises inside each single OUT placed in the reverberation chamber at 1, 1.8, 2.45, and 3 GHz are shown in Fig. 5 through Fig. 7. The measured temperature rise appeared to be higher at lower frequencies. This is due to the fact that the OUT's ACS decreases with frequency [16]. However, we observe that the temperature rise at 2.45 GHz is comparable to that at 1 GHz, which can be explained by the water molecules resonant behavior at this frequency. According to [24], the main ingredient of HSL is water, so this conclusion refers to the HSL-filled shell as well.

The ripple effects at 1 GHz are mainly due to the fact that the power coupled to the sphere changes as a function of paddle

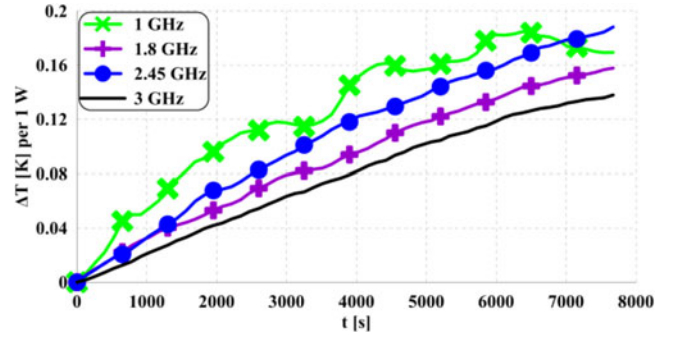


Fig. 5. Temperature rise measured inside water-filled small shell at four frequencies of interest, normalized to 1 W.

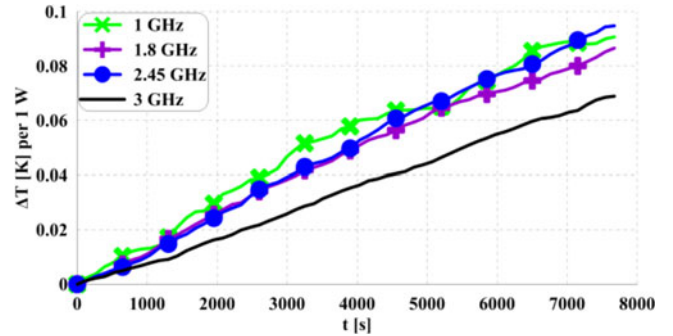


Fig. 6. Temperature rise measured inside water-filled large shell at four frequencies of interest, normalized to 1 W.

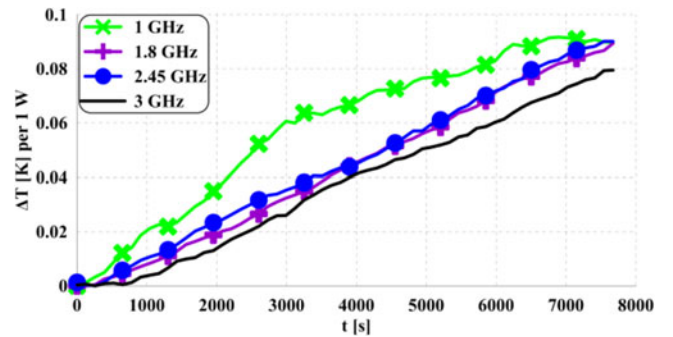


Fig. 7. Temperature rise measured inside HSL-filled large shell at four frequencies of interest, normalized to 1 W.

position, which is more prominent in the lower frequency range. This is directly related to the absorbed power distribution which is a function of the applied frequency, which will be shown at the end of this section.

According to (8) for temperature-based  $WBSAR$  measurements (i.e., calculated from the bio-heat equation), besides temperature rise, it is necessary to determine the convection heat transfer coefficient  $h$  of the OUT surrounded by air. This parameter was determined by measuring the temperature decrease due to the convective cooling of the heated liquid surrounded by air at room temperature. This measurement was performed inside the chamber with the RF power turned OFF. The measured temperature decrease, due to convection inside the reverberation

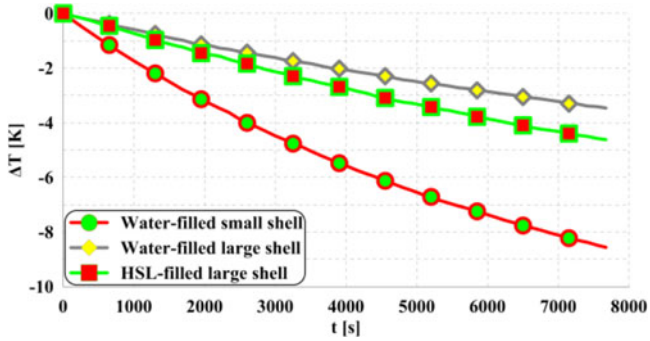


Fig. 8. Temperature decrease measurements due to convection.

TABLE I  
MEASURED CONVECTION HEAT TRANSFER COEFFICIENTS

OUT	Water-Filled Small Sphere	Water-Filled Large Shell	HSL-Filled Large Shell
$h$ [W/m <sup>2</sup> K]	8.4	8.3	9.1

chamber for three different OUTs, is shown in Fig. 8. Due to the fact that the cooling process is reversible, compared to the RF heating, measured temperatures are given as negative values. Clearly, the OUT's cooling properties depend on its size. Thus, the smaller object cools faster because it has a smaller heat capacity. The convection heat transfer coefficient [36 (p. 274)] was determined from measured liquid temperature decrease and ambient air temperature as:

$$h = \frac{\rho c V}{t A} \ln \frac{T_1 - T_0}{T_2 - T_0} \quad (17)$$

where  $A$  is the surface area between two media at different temperatures,  $V$  is the OUT's volume,  $T_1$  is the OUT's initial temperature,  $T_2$  is the cooled OUT's temperature,  $T_0$  is the surrounding air temperature, and  $t$  is the observed period of cooling.

The OUT's temperature was measured with three probes and the air temperature with one probe. Measurements were performed for a 2-h period, same as for the heating measurements. Convection heat transfer coefficients for the three different OUTs calculated with (17) are given in Table I.

$WBSAR$  values were calculated from measured temperature results with (8). Results for each single object exposed to high field levels at 1, 1.8, 2.45, and 3 GHz are shown in Fig. 9. We observe the highest  $WBSAR$  for the water-filled small shell, which was expected since the same OUT had the largest temperature rise in the 2-h exposure period. Similar to temperature results,  $WBSAR$  was the highest at 1 and 2.45 GHz.

Above, we calculated  $WBSAR$  in three different OUTs based on temperature measurements and bio-heat (8). The main goal of this study is to compare measured  $WBSAR$  results with theoretical ones derived from the *power balance theory* (14). From (14) we see that, besides the power transmitted inside the chamber, the exposure assessment in terms of  $WBSAR$  will be influenced by the chamber  $Q$ . Therefore, the exposure assessment in reflective environments should be based on a thorough

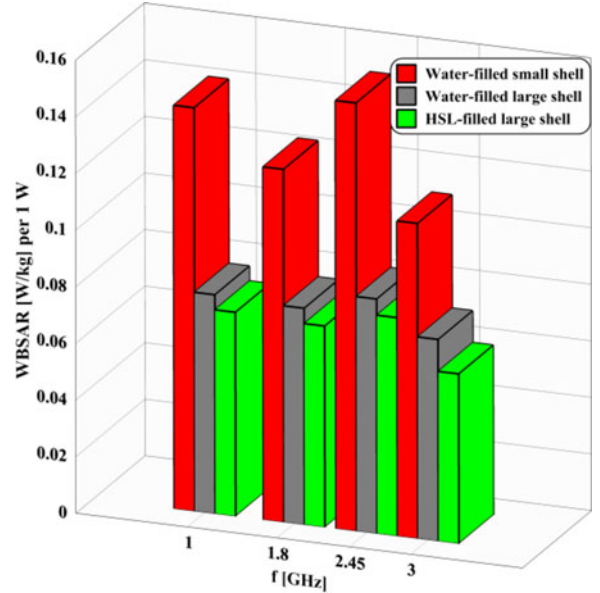


Fig. 9. Average  $WBSAR$  comparison of three different OUTs at four frequencies of interest, normalized to 1 W.

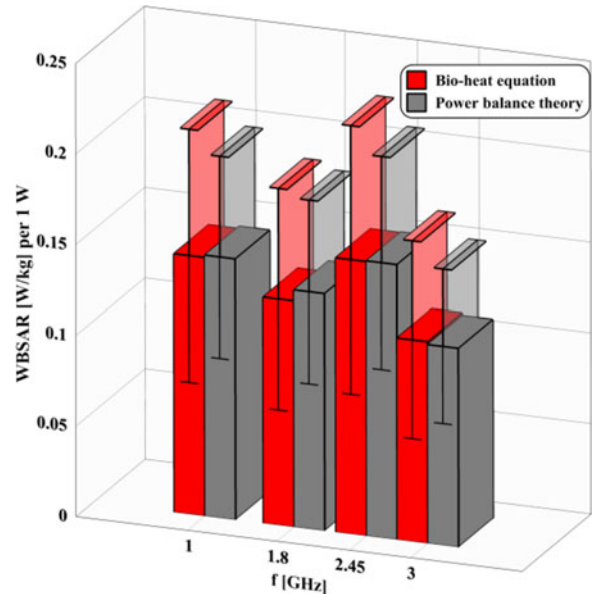


Fig. 10. Comparison of  $WBSAR$  measurements and theoretical assessment with error bars presenting combined uncertainty, normalized to 1 W for water-filled small shell.

environment characterization in terms of its  $Q$  factor. The  $WBSAR$  results based on the *power balance theory* (14), where the ACS results of the OUTs can be found in [16], along with  $WBSAR$  results from the bio-heat equation are given in Fig. 10 through Fig. 12. Excellent agreement between the two approaches can be seen within 5%  $\sim 0.2$  dB difference and especially within uncertainty given in Section VI for all tested OUTs and at each observed frequency. This clearly demonstrates that the *power balance theory* can be used for exposure assessment inside high- $Q$  environments.

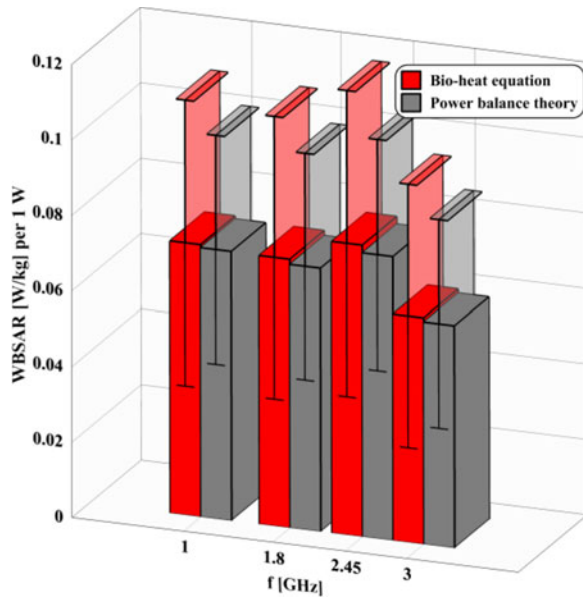


Fig. 11. Comparison of WBSAR measurements and theoretical assessment with error bars presenting combined uncertainty, normalized to 1 W for water-filled large shell.

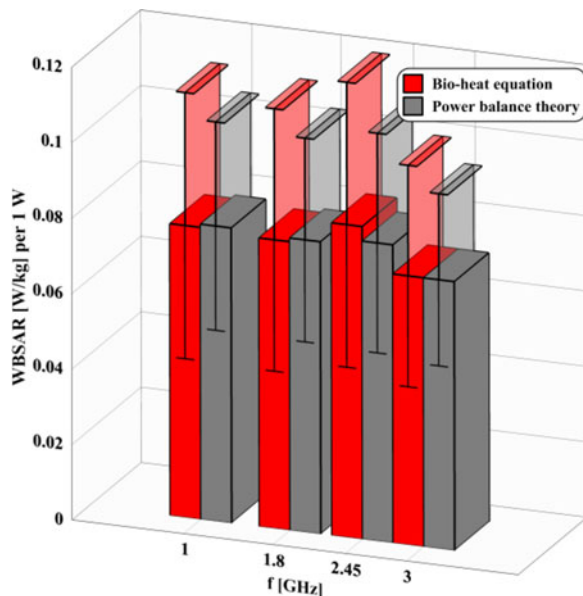


Fig. 12. Comparison of WBSAR measurements and theoretical assessment with error bars presenting combined uncertainty, normalized to 1 W for HSL-filled large shell.

We showed that the approach works for spherical shells filled with different lossy liquids, but it can also be applied for human exposure assessment. The main advantage of this approach is that it does not require any kind of invasive measurements. According to (14), it requires the knowledge of: 1) the environment's  $Q$ , which can be either measured or estimated, 2) the environment's volume, 3) the exposed object's ACS, which is well studied for humans, 4) the exposed object's mass, 5) the applied frequency, and 6) the transmitted power.  $Q$  and ACS

TABLE II  
 $Q$  AND ACS VALUES FROM [16]

	$f$ [GHz]	Water-Filled Small Sphere	Water-Filled Large Shell	HSL-Filled Large Shell
$Q_{\text{empty}}$	1		1900	
	1.8		2900	
	2.45		3230	
	3		3420	
$Q_{\text{loaded}}$	1	1350	980	890
	1.8	2400	2000	1900
	2.45	2650	2260	2210
	3	3000	2660	2500
ACS [m <sup>2</sup> ]	1	0.011	0.026	0.031
	1.8	0.007	0.015	0.017
	2.45	0.009	0.017	0.018
	3	0.006	0.013	0.017

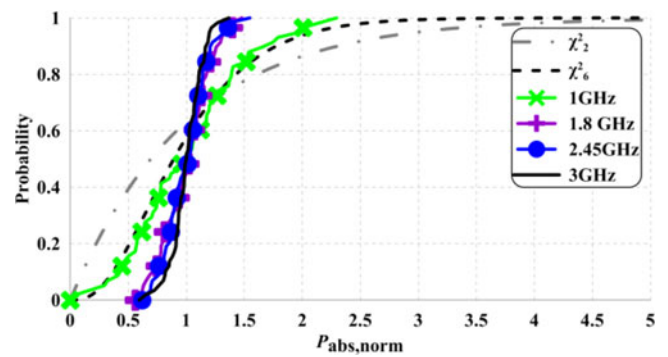


Fig. 13. CDF of the normalized power absorbed by the OUT.

values measured in [16] at four frequencies of interest are given in Table II.

In Fig. 5 through Fig. 7, we notice that temperature rise at 1.8, 2.45, and 3 GHz is almost linear, while the line representing 1 GHz shows some fluctuations. This can be explained by calculating the cumulative distribution function (CDF) at each frequency and comparing them with expected theoretical values.

Note that, ideally, each component of the electric field coupled to an electrically-small receiving antenna has a chi distribution ( $\chi$ ) with 2 degrees of freedom (DOF) ( $\chi_2$ ), while the total electric field has  $\chi$  distribution with 6 DOF ( $\chi_6$ ). Since power is proportional to the square value of the electric field, each power component coupled to the electrically-small receiving antenna is chi-squared distributed with 2 DOF ( $\chi_2^2$ ). Similarly, total power coupled to the antenna is chi-squared distributed with 6 DOF ( $\chi_6^2$ ).

Next, we calculate the CDF of the power absorbed by the OUTs at each frequency and compare it to the theoretical values. The CDF is the probability that the variable  $X$  takes a value less than or equal to  $x$ , i.e.,  $F(x) = \Pr(X \leq x)$ . The results are shown in Fig. 13. We notice that the CDF at 1 GHz calculated from measured absorbed power agrees well with theoretical  $\chi_6^2$  CDF, which was expected since objects appear electrically smaller at lower frequencies. Three other frequencies have similar CDFs calculated from measured absorbed power and agree with theoretical  $\chi_N^2$  CDF with  $N$  DOF. Note that  $\chi_N^2$  approaches

to the uniform distribution as  $N$  gets large [37]. Hence, we can conclude that at 1 GHz, the absorbed power distribution is similar to  $\chi_6^2$ , while at the other three frequencies the absorbed power distribution is similar to  $\chi_N^2$  with large numbers of DOF approaching uniform distribution. This conclusion is in a good agreement with observed characteristics of the OUTs temperature rise, where larger fluctuations were observed at 1 GHz while other frequencies exhibited almost uniform power distribution and temperature rise.

## VI. MEASUREMENT UNCERTAINTY

Since two different setups were used to determine *WBSAR*, it is useful to give the uncertainty budget for both setups. The setup used for the exposure assessment, based on *power balance theory*, was the same one used in [16] to calculate the *ACS*. The obtained expanded uncertainty was  $\pm 2.84$  dB.

Before calculating the uncertainty for the bio-heat-equation-based exposure assessment, the contribution factors need to be identified. There are five dominant factors influencing the measured quantity. The spatial field distribution inside the reverberation chamber is assumed to be uniform if the standard deviation is lower than 3 dB. However, even if the standard deviation is below that limit, we cannot assume a completely uniform field distribution, meaning that some parts of the OUTs can be exposed to the higher field levels than the others. For this reason we need to perform a chamber calibration in order to determine the influence of spatial field uniformity (*SU*) on the measured quantity. *SU* presents an uncertainty contribution factor for both, the bio-heat equation based and *power balance theory* based *WBSAR* assessment.

In [16] and Section IV-B, we measured the *SU* below 1.4 dB. In the bio-heat-equation-based exposure assessment the *WBSAR* was determined by measuring the lossy material temperature rise due to the high-field exposure. The fluoroptic thermometer has an accuracy (*TA*) of  $\pm 0.5$  K in the observed temperature range [25]. A temperature change inside the lossy object of  $\pm 0.5$  K causes a *WBSAR* change of  $\pm 0.97$  dB (*TA-SAR*). Additionally, the same thermometer was used for calculating the convective heat transfer coefficient  $h$ , and  $\pm 0.5$  K change of temperature measurements causes a change of the convective heat transfer coefficient which results in a change of assessed *WBSAR* of  $\pm 0.22$  dB (*TA-h*). To determine the *WBSAR*, we measured the power coupled to the chamber. In the proposed measurements, power was measured by a power sensor connected to the power meter. An uncertainty estimated from manufacturer specifications for the used power monitoring devices was  $\pm 0.1$  dB (*PM*). Losses inside the cables used for this setup were measured with the VNA whose accuracy was  $\pm 0.2$  dB. The VNA was calibrated with an electronic calibration module (*E-cal*) which has its own uncertainty of  $\pm 0.1$  dB. The uncertainty budget for the bio-heat-equation-based exposure assessment is given in Table III. The obtained expanded uncertainty equals  $\pm 3.47$  dB. The achieved uncertainties of both methods are comparable to the expected uncertainty of field measuring instruments, which are commonly used to assess the human exposure to EM fields, according to [38 (p. 46)]. Note that the given uncertainty

TABLE III  
MEASUREMENTS UNCERTAINTY BUDGET

Uncertainty Source	<i>SU</i>	<i>TA-SAR</i>	<i>TA-h</i>	<i>PM</i>	VNA	<i>E-Cal</i>
Uncertainty [dB]	1.4	0.97	0.22	0.1	0.2	0.1
Combined Uncertainty						1.73 dB
Expanded ( $k = 2$ ) Uncertainty						3.47 dB

estimation is conservative. The *SU* was determined in the Cartesian field, even though the *WBSAR* actually depends on the total field, which generally has smaller variations. Therefore, true measurement uncertainty is likely lower than that given in Table III.

## VII. CONCLUSION

In this paper, we presented an approach for exposure assessment due to the RF electromagnetic fields inside indoor reverberant environments without the need for electromagnetic field (EMF) measurements. The approach based on the *power balance theory* was consistent with experimental results obtained from measured temperature increases inside lossy objects exposed to the EMF inside the reverberation chamber. Excellent agreement, within measurement uncertainty, between the proposed novel approach based on the *power balance theory* and one based on the bio-heat equation confirmed its validity.

The method presented for exposure assessment can be applied to humans without the need to perform invasive measurements. Exposure assessment was given in terms of the *WBSAR* as a basic restriction quantity given in relevant exposure limiting standards. The exposure assessment was based on the environment's  $Q$  factor, an important parameter that characterizes any reverberant environment, and *ACS* as a key parameter describing the lossy object's absorption characteristics.

## REFERENCES

- [1] D. A. Hill, *Electromagnetic fields in cavities*, Piscataway, NJ, USA: Wiley, 2009.
- [2] International Commission on Non-Ionizing Radiation Protection [IC-NIRP]. "Guidelines for limiting exposure to time-varying electric, magnetic, and electromagnetic fields [up to 300 GHz]," *Health Phys.* vol. 74, pp. 494–522, 1998.
- [3] *IEEE Standard for Safety Levels with Respect to Human Exposure to Radio Frequency Electromagnetic Fields, 3 kHz to 300 GHz*, IEEE C95.1-2005, 2006.
- [4] A. Bamba *et al.*, "Experimental assessment of specific absorption rate using room electromagnetics," *IEEE Trans. Electromagn. Compat.*, vol. 54, no. 4, pp. 747–757, Aug. 2012.
- [5] G. Vermeeren, W. Joseph, C. Olivier, and L. Martens, "Statistical multipath exposure of a human in a realistic electromagnetic environment," *Health Phys.*, vol. 94, no. 4, pp. 345–354, Apr. 2008.
- [6] A. Bamba, W. Joseph, E. Tanghe, G. Vermeeren, and L. Martens, "Circuit model for diffuse multipath and electromagnetic absorption prediction in rooms," *IEEE Trans. Antennas Propag.*, vol. 61, no. 6, pp. 3292–3301, Jun. 2013.
- [7] H. Kuttruff, *Room Acoustics*, London, U.K.: Spon Press, 2000.
- [8] R. Habash, *Electromagnetic Fields and Radiation*. New York, NY, USA: CRC Press, 2001.
- [9] H.H. Pennes, "Analysis of tissue and arterial blood temperatures in the resting human forearm," *J. Appl. Physiol.*, vol. 1, no. 2, pp. 5–34, Aug. 1948.

[10] Y. Xuan and W. Roetzel, "Bioheat equation of the human thermal system," *Chem. Eng. Technol.*, vol. 20, no. 4, pp. 268–276, May 1997.

[11] D. Senic *et al.*, "Estimating and reducing uncertainty in reverberation-chamber characterization at millimeter-wave frequencies," *IEEE Trans. Antennas Propag.*, vol. 64, no. 7, pp. 3130–3140, Jul. 2016.

[12] P.-S. Kildal, X. Chen, C. Orlenius, M. Franzen, and C. L. Patané, "Characterization of reverberation chambers for OTA measurements of wireless devices: Physical formulations of channel matrix and new uncertainty formula," *IEEE Trans. Antennas Propag.*, vol. 60, no. 8, pp. 3875–3891, Aug. 2012.

[13] C. Lemoine, E. Amador, and P. Besnier, "On the  $K$ -factor estimation for Rician channel simulated in reverberation chamber," *IEEE Trans. Antennas Propag.*, vol. 59, no. 3, pp. 1003–1012, Mar. 2011.

[14] D. Senic, "Human exposure and wireless communication aspects of electromagnetic wave absorption in dissipative objects inside reverberant environments," Ph.D. Dissertation, FESB, Univ. Split, Split, Croatia, 2014.

[15] A. Sarolic and D. Senic, "Novel method for practical SAR determination in indoor exposure scenarios without the need for EMF measurements, based on reverberation chamber theory," in *Proc. 2015 Annu. Meet. Bioelectromag.*, USA, Jun. 2015, pp. 324–328.

[16] D. Senic, A. Sarolic, J. M. Joskiewicz, and C. L. Holloway, "Absorption cross-section measurements of a human model in a reverberation chamber," *IEEE Trans. Electromagn. Compat.*, vol. 58, no. 3, pp. 721–728, Jun. 2016.

[17] D. Senic, A. Sarolic, and Z. M. Joskiewicz, "Preliminary results of human body average absorption cross section measurements in reverberation chamber," in *Proc. Int. Symp. Electromagn. Compat.*, 2013, pp. 887–890.

[18] D. Senic, C. L. Holloway, J. M. Ladbury, G. H. Koepke, and A. Sarolic, "Absorption characteristics and SAR of a lossy sphere inside a reverberation chamber," in *Proc. Int. Symp. Electromagn. Compat.*, 2014, pp. 962–967.

[19] G. C. R. Melia, I. D. Flintoft, and M. P. Robinson, "Absorption cross-section of the human body in a reverberant environment," *EMC Eur.*, Rome, Italy, Sep. 2012, pp. 1–6.

[20] I. D. Flintoft, G. C. R. Melia, M. P. Robinson, J. F. Dawson, and A. C. Marvin, "Rapid and accurate broadband absorption cross-section measurement of human bodies in a reverberation chamber," *IOP Meas. Sci. Technol.*, vol. 26, no. 6, Jun. 2015, Art. no. 065701.

[21] I. D. Flintoft, M. P. Robinson, G. C. R. Melia, J. F. Dawson, and A. C. Marvin, "Average absorption cross-section of the human body measured at 1–12 GHz in a reverberant environment: Results of a human volunteer study," *IOP Phys. Med. Biol.*, vol. 59, no. 13, pp. 3297–3317, July 2014.

[22] Electromagnetic Compatibility (EMC) – Part 4-21: Testing and measurements techniques – Reverberation chamber test methods, IEC 61000-4-21, May 2005.

[23] J. Ladbury, G. Koepke, and D. Camell, "Evaluation of the NASA Langley research center mode-stirred chamber facility," Nat. Inst. Standards Technol., Boulder, CO, USA, Tech. Rep. 1508, 1999.

[24] *CTIA Broadband Fluid Batch No. CTIA 3.2. IndexSAR Ltd.*, Newdigate, U.K., 2013.

[25] *Model 3100, 3101, and 3102 Fluoroptic Thermometer User Manual*. Luxtron Corp., Santa Clara, CA, USA, 2003.

[26] *Hart scientific 1522—Handheld thermometer*. Fluke Corp., Washington, DC, USA, 2005.

[27] K. G. Beauchamp and C. K. Yuen, *Digital Methods for Signal Analysis*, London, U.K.: Allen, 1976.

[28] K. Rosengren, P.-S. Kildal, C. Carlsson, and J. Carlsson, "Characterization of antennas for mobile and wireless terminals in reverberation chambers: Improved accuracy by platform stirring," *Microw. Opt. Technol. Lett.*, vol. 30, no. 6, pp. 391–397, Sep. 2001.

[29] K. Madsen, P. Hallbjørner, and C. Orlenius, "Models for the number of independent samples in reverberation chamber measurements with mechanical, frequency, and combined stirring," *IEEE Antenn. Propagat. Lett.*, vol. 3, no. 1, pp. 48–51, Dec. 2004.

[30] O. Lunden and M. Backstrom, "Stirrer efficiency in FOA reverberation chambers: Evaluation of correlation coefficients and chi-squared tests," in *Proc. IEEE Int. Symp. Electromagn. Compat.*, Aug. 2000, vol. 1, pp. 11–16.

[31] C. L. Holloway, D. A. Hill, J. M. Ladbury, P. F. Wilson, G. H. Koepke, and J. Coder, "On the use of reverberation chambers to simulate a Rician radio environment for the testing of wireless devices," *IEEE Trans. Antennas Propag.*, vol. 54, no. 11, pp. 3167–3177, Nov. 2006.

[32] C.-M. Wang *et al.*, "Parameter estimation and uncertainty evaluation in a low Rician  $K$ -factor reverberation-chamber environment," *IEEE Trans. Electromagn. Compat.*, vol. 56, no. 5, pp. 1002–1012, Oct. 2014.

[33] P.-S. Kildal, X. Chen, C. Orlenius, M. Franzen, and C. L. Patané, "Characterization of reverberation chambers for OTA measurements of wireless devices: Physical formulations of channel matrix and new uncertainty formula," *IEEE Trans. Antennas Propag.*, vol. 60, no. 8, pp. 3875–3891, Aug. 2012.

[34] C. Lemoine, E. Amador, and P. Besnier, "On the  $K$ -factor estimation for Rician channel simulated in reverberation chamber," *IEEE Trans. Antennas Propag.*, vol. 59, no. 3, pp. 1003–1012, Mar. 2011.

[35] K. A. Remley *et al.*, "Configuring and verifying reverberation chambers for testing cellular wireless devices," *IEEE Trans. Electromagn. Compat.*, vol. 58, no. 3, pp. 661–672, Jun. 2016.

[36] J. R. Welty, C. E. Wicks, R. E. Wilson, and G. L. Rorrer, *Fundamentals of Momentum, Heat, and Mass Transfer*. Hoboken, NJ, USA: Wiley, 2008.

[37] N. L. Johnson and S. Kotz, *Distributions in Statistics*. Hoboken, NJ, USA: Wiley, 1970.

[38] *IEEE Recommended Practice for Measurements and Computations of Radio Frequency Electromagnetic Fields With Respect to Human Exposure to Such Fields, 100 kHz–300 GHz*, IEEE C95.3-2002 2008.



**Damir Senic** (S'09–M'16) received the M.Sc. degree in 2008 and the Ph.D. degree in 2014, both in electrical engineering from University of Split, Faculty of Electrical Engineering, Mechanical Engineering and Naval Architecture, Split, Croatia.

He is currently with University of Colorado Boulder working at National Institute of Standards and Technology, Communications Technology Laboratory in Boulder as a Postdoctoral Research Associate through Professional Research Experience Program.

His research interests include millimeter wave radio-communications, electromagnetic measurements, electromagnetic compatibility (EMC) and bioeffects of EM fields.

Dr. Senic received Richard E. Merwin Award of the IEEE Computer Society for exemplary involvement in the IEEE Activities and Excellent Academic Achievement in 2013.



**Antonio Sarolic** (S'99–M'05) received the Ph.D. degree in electrical engineering from the University of Zagreb, Zagreb, Croatia, in 2004.

He joined the Faculty of Electrical Engineering, Mechanical Engineering and Naval Architecture, University of Split, Split, Croatia, in 2006, and is currently a Professor of electrical engineering, the Chair of applied electromagnetics, and the Head of Laboratory for EMC and EM Research at FESB. He is the proposer and the Chair of the ongoing European COST Action BM1309 (EMF-MED): "European network for innovative uses of electromagnetic fields (EMFs) in biomedical applications", 2014–2018.

He was the Project Leader of a recently completed research project "Measurements in EMC and EM health effects research" funded by the Croatian Ministry of Science, and currently leads the ongoing project "Measurements in bioelectromagnetics." He led or participated in several other research and development projects related to electromagnetic compatibility and applied electromagnetics, and has been involved in several related ongoing or completed EU COST Actions. He teaches a range of courses at FESB, related to applied electromagnetics, electromagnetic compatibility, antennas, wireless communications, and bioelectromagnetics.

Dr. Sarolic received the University Grant from the IEEE EMC Society, for developing the EMC course at FESB, in 2008. He is a member of the IEEE (EMC, AP, and EMB societies), the BEMS, and the EBEA, and has served as Chair of the IEEE EMC Society—Croatia Chapter for 4 years. He is the Chairman of the Croatian Standardization Technical Committee HZN TO E106 "Electromagnetic fields in human environment," and a member of the committee HZN TO E500 "Electromagnetic compatibility."



**Christopher L. Holloway** (S'86–M'92–SM'04–F'10) received the B.S. degree from the University of Tennessee, Chattanooga, TN, USA, in 1986, and the M.S. and Ph.D. degrees from the University of Colorado at Boulder, Boulder, CO, USA, in 1988 and 1992, respectively, both in electrical engineering.

During 1992, he was a Research Scientist with Electro Magnetic Applications, Inc., Lakewood, CO, USA. His responsibilities included theoretical analysis and finite-difference time-domain modeling of various electromagnetic problems. From the fall of 1992 to 1994, he was with the National Center for Atmospheric Research (NCAR) in Boulder. While at NCAR his duties included wave propagation modeling, signal processing studies, and radar systems design. From 1994 to 2000, he was with the Institute for Telecommunication Sciences, U.S. Department of Commerce in Boulder, where he was involved in wave propagation studies. Since 2000, he has been with the National Institute of Standards and Technology, Boulder, CO, USA, where he works on electromagnetic theory. He is also on the Graduate Faculty at the University of Colorado at Boulder. His research interests include electromagnetic field theory, wave propagation, guided wave structures, remote sensing, numerical methods, metamaterials, measurement techniques, EMC/EMI issues, and atom-based metrology.

Dr. Holloway is a member of the URSI Commissions A, B, and E. He is currently serving as a Chair for the US Commission A of the International Union of Radio Science and is an Associate Editor for the IEEE TRANSACTIONS ON ELECTROMAGNETIC COMPATIBILITY. He was the Chairman for the Technical Committee on Computational Electromagnetics (TC-9) of the IEEE Electromagnetic Compatibility Society from 2000–2005, served as a Cochair for the Technical Committee on Nano-Technology and Advanced Materials (TC-11) of the IEEE EMC Society from 2006–2011, and served as an IEEE Distinguished Lecturer for the EMC Society from 2004–2006.



**John M. Ladbury** was born in Denver, CO, USA, in 1965. He received the B.S.E.E. and M.S.E.E. degrees (specializing in signal processing) from the University of Colorado, Boulder, in 1987 and 1992, respectively.

Since 1987, he has been working on EMC metrology and facilities with the Radio Frequency Technology Division, of N.I.S.T., Boulder, CO, USA. His main research interests include reverberation chambers, with some investigations into other EMC-related topics such as time-domain measurements and probe calibrations. He was involved with the revision of RTCA DO160D and is a member of the IEC joint task force on reverberation chambers.

Mr. Ladbury received four “Best Symposium Paper” awards at the IEEE International EMC symposia, a Technical Achievement Award from the IEEE EMC society for significant contributions in the development of reverberation chamber techniques for EMC applications, and the US Department of Commerce Bronze Medal for his research in reverberation chambers.